Pergamon

Int. J. Heat Mass Transfer. Vol. 40, No. 16, pp. 3861–3873, 1997

Printed in Great Britain
0017-9310/97 $17.00+0.00

PII: S0017-9310(97)00042-2

Developing turbulent convective heat transfer in helical pipes

C. X. LIN and M. A. EBADIAN†

Florida International University, Hemispheric Center for Environmental Technology, Miami, FL 33199, U.S.A.

(*Received* 29 *April* 1996 *and in final form* 14 *January* 1997)

Abstract—A fully elliptic numerical study has been carried out to investigate three-dimensional turbulent developing convective heat transfer in helical pipes with finite pitches. The k–ε standard two-equation turbulence model is used to simulate turbulent flow. The governing equations are solved by a control-volume finite element method. Numerical results have been compared to the existing experimental data and a good agreement has been obtained. The results presented in this paper cover a Reynolds number range of $2.5 \times 10^4 \sim 1.0 \times 10^5$, a pitch range of $0.0 \sim 0.6$ and a curvature ratio range of $0.025 \sim 0.050$. The developments of effective thermal conductivity and temperature fields and local and average Nusselt numbers are given and discussed. It has been found that the examined parameters exert complex effects on developing thermal fields and heat transfer in the helical pipes. The Nusselt numbers for the helical pipes are oscillatory before the flow is fully developed, especially for the case of relatively large curvature ratio.

INTRODUCTION

Forced convection heat transfer in helical pipes with a constant circular cross-section is of importance in piping systems, heat exchangers, storage tanks, chemical reactors and many other engineering applications. Due to the occurrence of a secondary flow in planes normal to the main flow, heat transfer in helical pipes differs significantly from that in straight pipes. Berger *et al.* [1] and Shah and Joshi [2] have reviewed the literature on fluid flow and heat transfer in helical pipes. A recent survey of the literature on convection heat transfer in helical pipes by the present authors indicates that most of the previous studies on this subject were performed within the laminar flow region. In contrast, the literature available in open publications on turbulent heat transfer in helical pipes is relatively sparse.

Experimental studies of turbulent heat transfer in helical pipes have been conducted by Seban and McLaughlin [3], Rogers and Mayhew [4], Hogg [5], Mori and Nakayama [6], Kalb and Seader [7], Mikaila and Poskas [8], and Rao [9, 10]. These studies were carried out within zero or very small pitch ranges and the data mainly encompassed fully developed average Nusselt numbers. Among the numerical studies, Patankar *et al.* [11] applied the standard k–ε two-equation turbulence model to predict the turbulent developing fluid flow in curved pipes. As to helical pipes, only fully developed hydrodynamic results at zero pitch were reported in their study. Yang and Ebadian [12] adopted the same turbulence model to investigate fully developed turbulent heat transfer in helical pipes with substantial pitch. Both of these numerical studies employed the control-volume-based finite difference method developed by Patankar and Spalding [13], a method which is of first-order accuracy. These two studies also treated the flow as parabolic; the diffusion fluxes in the axial direction together with terms of small order of magnitude in governing equations were neglected. As the turbulent flow inside helical pipes was fully three-dimensional, the parabolic computation may lead to results of low accuracy or reliability. To the authors' knowledge, no data is available in open literature concerning the turbulent developing heat transfer in helical pipes, especially those with finite pitch.

In this paper, turbulent developing heat transfer in helical pipes with finite pitch is investigated with the standard k–ε turbulence model. To capture the physics of the flow and heat transfer, fully elliptic flow calculations have been performed with a control-volume finite element method (CVFEM) of second-order accuracy. The effects of pitch, curvature ratio and Reynolds number on the developments of effective thermal conductivity and temperature fields, and local and average Nusselt numbers are examined.

PHYSICAL PROBLEM

The geometry and system of coordinates considered are shown in Fig. 1. The circular pipe studied, which has a diameter of $2a$, is coiled at a radius of R_c with the distance between two turns (the pitch) represented as H. The orthogonal helical coordinate system (s, r, θ) or (s, η, ζ) in reference to the master Cartesian coor-

† Author to whom correspondence should be addressed.

NOMENCLATURE

a radius of the helical pipe [m]
A area [m^2]
A_T Van Driest constant
b intermediate parameter [m^{-1}]
$C_{\varepsilon 1} C_{\varepsilon 2} C_\mu$ turbulence model constants
d_h hydraulic diameter of the helical pipe [m]
E empirical constant in logarithmic velocity profile
H pitch [m]
I turbulence intensity ($=u'/u \times 100\%$)
k turbulent kinetic energy [$m^2 s^{-2}$]
L characteristic turbulence length scale [m]
n coordinate direction perpendicular to a surface
Nu_m circumferential average Nusselt number on a cross-section ($=(1/2\pi)\int_0^{2\pi} Nu_\theta \, d\theta$)
Nu_θ local Nusselt number on the circumference of a pipe ($=(q_w d_h/\Gamma_l)/(T_w - T_b)$)
p pressure [Nm^{-2}]
Pr molecular Prandtl number
Pr_w turbulent wall Prandtl number
q_w local heat flux [Wm^{-2}]
r radial coordinate [m]
R_c radius of the coil [m]
Re Reynolds number ($=\rho u_0 d_h/\mu$)
s axial coordinate [m]
T temperature [K]
T_b fluid bulk temperature on one cross-section ($=(1/\bar{u}_s A)\int_0^A u_s T \, dA$) [K]
u velocity component in flow direction [ms^{-1}]
u' root-mean-square turbulent velocity fluctuation [ms^{-1}]
u_0 inlet velocity [$m^{-1}s$]
u_i velocity component in i-direction ($i = 1, 2, 3$) [$m\,s^{-1}$]
u^* friction velocity ($=\sqrt{\tau_w/\rho}$) [ms^{-1}]
X, Y, Z master Cartesian coordinates [m]
x_i Cartesian coordinate in i-direction ($i = 1, 2, 3$) [m].

Greek symbols
α angle [°]
Γ thermal conductivity [$W(m \cdot K)^{-1}$]
Γ_{eff} effective thermal conductivity [$W(m \cdot K)^{-1}$]
δ curvature ratio ($=a/R_c$)
δ_{ij} Dirac delta function
ε dissipation rate of turbulent kinetic energy [$m^2 s^{-3}$]
η, ζ orthogonal rectangular coordinate [m]
φ axial angle [°]
κ Von Karman constant
λ nondimensional pitch ($=H/(2\pi R c)$)
μ viscosity [$kg(m \cdot s)^{-1}$]
θ orthogonal azimuthal coordinate [°]
Θ nondimensional temperature ($=(T - T_w)/(T_b - T_w)$)
ρ density of fluid [$kg\,m^{-3}$]
σ_τ turbulent Prandtl number in energy equation
σ_k diffusion Prandtl number for k
σ_ε diffusion Prandtl number for ε
τ_w wall shear stress [$N\,m^{-2}$].

Subscripts
0 inlet conditions
b bulk quantity
i, j, k general spatial indices
l laminar or molecular quantity
r, θ, s radial, azimuthal and axial directions, respectively
t turbulent quantity
w wall condition.

Superscripts
$+$ standard wall coordinates
$-$ average quantity.

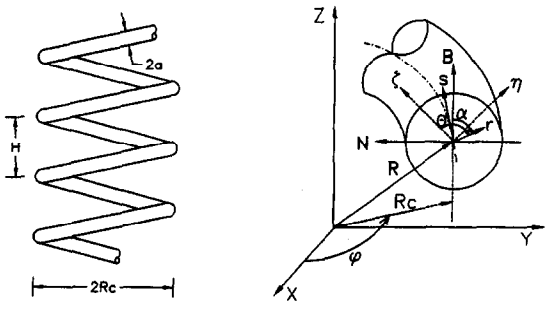

(a) (b)

Fig. 1. Geometry and system of coordinates: (a) helical pipe; (b) helical coordinate system.

dinate system **X** (X, Y, Z) is similar to that used by Germano [14] and Liu [15] with

$$\theta = \alpha + \frac{H}{2\pi} s b^2 + \theta_0 \tag{1}$$

where $\theta_0 =$ constant and $b = [R_c^2 + (H/2\pi)^2]^{-1/2}$. A given point in the helical pipe can be mapped to the master Cartesian system through

$$\mathbf{X} = \mathbf{R} + r\cos\alpha \mathbf{N} + r\sin\alpha \mathbf{B} \tag{2}$$

$$\mathbf{R} = \left(R_c \cos\varphi, R_c \sin\varphi, \frac{H}{2\pi}\varphi\right) \tag{3}$$

$$\mathbf{N} = (-\cos\varphi, -\sin\varphi, 0) \tag{4}$$

$$\mathbf{B} = \left(\frac{H}{2\pi} b \sin\varphi, \frac{H}{2\pi} b \cos\varphi, bR_c\right) \tag{5}$$

where **R** is the global coordinate vector at a point on the center line of the helical pipe and **N** and **B** are the normal and binomial to the center line at the point of consideration.

At the inlet ($\varphi = 0°$), fluid with turbulence intensity I and temperature T_0 enters into the helical pipe at a speed of u_0. The wall of the pipe is heated under constant temperature T_0. Turbulent flow and heat transfer develop simultaneously downstream in the pipe. The flow is assumed to be steady and incompressible. The k–ε turbulence model of Launder and Spalding [16] is used to simulate turbulent flow. The Reynolds stresses are related to the mean velocity gradients on the basis of the Boussinesq hypothesis. The turbulent heat flux in the energy equation is modeled using the gradient transport analogy. The time-averaged, fully elliptic differential equations governing the turbulent flow in helical pipe can be written in tensor form as

Mass

$$\frac{\partial u_j}{\partial x_i} = 0. \tag{6}$$

Momentum

$$\frac{\partial}{\partial x_j}\left[(\mu_l + \mu_t)\left(\frac{\partial u_i}{\partial x_j} + \frac{\partial u_j}{\partial x_i} - \delta_{ij}\frac{2}{3}\frac{\partial u_k}{\partial x_k}\right) - \rho u_j u_i - \delta_{ij} p\right] = 0. \tag{7}$$

Energy

$$\frac{\partial}{\partial x_j}\left[\left(\Gamma_l + \frac{\mu_t C_p}{\sigma_\tau}\right)\frac{\partial T}{\partial x_j} - \rho u_j C_p T\right] + \mu_l \Phi_v + \rho\varepsilon = 0. \tag{8}$$

Turbulent kinetic energy

$$\frac{\partial}{\partial x_j}\left[\left(\mu_l + \frac{\mu_t}{\sigma_k}\right)\frac{\partial k}{\partial x_j} - \rho u_j k\right] + \rho P - \rho\varepsilon = 0. \tag{9}$$

Dissipation rate of turbulent kinetic energy

$$\frac{\partial}{\partial x_j}\left[\left(\mu_l + \frac{\mu_t}{\sigma_\varepsilon}\right)\frac{\partial \varepsilon}{\partial x_j} + \rho u_j \varepsilon\right] + C_{\varepsilon 1}\frac{\rho\varepsilon P}{k} - C_{\varepsilon 2}\frac{\rho\varepsilon^2}{k} = 0 \tag{10}$$

where

$$P = \frac{\mu_t}{\rho}\frac{\partial u_i}{\partial x_j}\left(\frac{\partial u_i}{\partial x_j} + \frac{\partial u_j}{\partial x_i}\right) \tag{11}$$

$$\Phi_v = \frac{\partial u_i}{\partial x_j}\left(\frac{\partial u_i}{\partial x_j} + \frac{\partial u_j}{\partial x_i} - \frac{2}{3}\frac{\partial u_k}{\partial x_k}\delta_{ij}\right). \tag{12}$$

In the above equations, the subscripts $i, j, k = 1, 2, 3$. Turbulent kinetic energy, k and its dissipation rate, ε, are coupled to the governing equations via the relation $\mu_t = \rho C_\mu k^2/\varepsilon$. In the Cartesian system, x_1, x_2 and x_3 correspond to X, Y and Z, respectively. The empirical constants for the turbulence model are assigned the following values in accordance with the recommendation of Launder and Spalding [16]:

$$C_\mu = 0.09, \quad C_{\varepsilon 1} = 1.47, \quad C_{\varepsilon 2} = 1.92,$$
$$\sigma_\tau = 0.7, \quad \sigma_k = 1.0, \quad \sigma_\varepsilon = 1.3.$$

A nonslip boundary condition is imposed on the wall of the helical pipe. The two-layer based non-equilibrium wall function method [17] is used to account for the near wall regions in the numerical computation of turbulent flow. The first near wall numerical grid point, M, is located sufficiently far from the wall for the local turbulent Reynolds number ($= \rho k^{1/2} l/\mu$, where $l = k^{3/2}/\varepsilon$) to be much greater than unity. In the region between the wall and node M, the expression for velocity is:

$$\frac{u}{u^*} = \begin{cases} y^+ & y^+ \leqslant y_v^+ \\ \dfrac{1}{\kappa}\ln(Ey^+), & y^+ > y_v^+ \end{cases}. \tag{13}$$

Here, u and y denote the velocity component in flow direction and the normal distance from the wall, respectively. The term y^+ is the dimensionless y ($y^+ = \rho u^* y/\mu$); $\kappa = 0.41$; and $E = 9.793$ (for a smooth wall). The term y_v^+ represents the thickness of the viscous sublayer ($y^+ = 11.225$). Outside of the viscous sublayer, the friction velocity, defined as $\sqrt{\tau_w/\rho}$ is computed as $u^* = C_\mu^{1/4} k^{1/2}$.

In the near wall cell, the value of the dissipation rate of the turbulent kinetic energy is given by:

$$\varepsilon = \frac{C_\mu^{3/4} k^{3/2}}{\kappa y}. \tag{14}$$

The turbulent kinetic energy equation is solved with zero normal derivative wall boundary conditions. The production term is computed using the velocity wall function described above to compute wall shear stress, and the dissipation at the near wall cell is obtained using an average over the cell:

$$\bar{\varepsilon} = \frac{C_\mu^{1/2} uk}{y}. \tag{15}$$

The wall heat flux is computed using $q_w = \rho C_p u^* \Delta T/T^+$, where T^+ is obtained from

$$T^+ = \begin{cases} Pr\dfrac{u}{u^*}, & y^+ \leqslant y_v^+ \\ Pr_w\left(\dfrac{u}{u^*} + P_T\right), & y^+ > y_v^+ \end{cases} \tag{16}$$

$$P_T = \frac{\pi/4}{\sin(\pi/4)}\left(\frac{A_T}{\kappa}\right)^{1/2}\left(\frac{Pr}{Pr_w} - 1\right)\left(\frac{Pr_w}{Pr}\right)^{1/4} \tag{17}$$

where Pr is the molecular Prandtl number; Pr_w, the turbulent wall Prandtl number ($Pr_w = 1.2$); and A_T, the Van Driest constant ($A_T = 26$).

At the inlet, uniform profiles for all the dependent variables are employed:

$$u_s = u_0, \quad u_r = 0, \quad u_\theta = 0,$$
$$T = T_0, \quad k = k_0, \quad \varepsilon = \varepsilon_0 \tag{18}$$

where u_s, u_r and u_θ are the axial, radial and azimuthal velocities, respectively. Turbulent kinetic energy at the inlet, k_0, and the dissipation rate of turbulent kinetic energy at the inlet, ε_0, are estimated by

$$k_0 = \frac{3}{2}(u_0 I)^2, \quad \varepsilon_0 = C_\mu^{3/4}\frac{k^{3/2}}{L}. \tag{19}$$

In equation (19), the turbulence intensity level, I, is defined as $u'/u \times 100\%$. As the turbulent eddies cannot be larger than the pipe, the turbulence characteristic length scale, L, is set to be $0.07a$ in the present study. The factor of 0.07 is based on the maximum value of the mixing length in fully developed turbulent pipe flow.

At the outlet, the diffusion flux for all variables in exit direction are set to be zero:

$$\frac{\partial}{\partial n}(u_s, u_r, u_\theta, T, k, \varepsilon) = 0. \tag{20}$$

To represent results, the following nondimensional variables and parameters are defined:

$$Re = \frac{\rho u_0 d_h}{\mu}, \quad \delta = \frac{a}{R_c}, \quad \lambda = \frac{H}{2\pi R_c}$$

$$T_b = \frac{1}{\bar{u}_s A}\int_0^A u_s T \, dA, \quad \Theta = \frac{T - T_w}{T_b - T_w}$$

$$Nu_\theta = \frac{q_w d_h}{\Gamma_l (T_w - T_b)}, \quad Nu_m = \frac{1}{2\pi}\int_0^{2\pi} Nu_\theta \, d\theta \tag{21}$$

where δ is the curvature ratio; λ, nondimensional pitch; Nu_θ the local Nusselt number along the circumference of the pipe; and Nu_m, the circumferential average Nusselt number on one cross-section. The term Θ represents nondimensional temperature, while T_b and u_s denote fluid bulk temperature and average axial velocity on one cross-section. Effective thermal conductivity is defined as:

$$\Gamma_{eff} = \Gamma_l + \frac{\mu_t C_p}{\sigma_\tau}. \tag{22}$$

It is known that, the critical Reynolds number identifying a transition from laminar to turbulent flow, Re_{crit}, is much higher in a curved pipe than in a straight pipe. According to Srinivasan *et al.* [18], Re_{crit} can be estimated by

$$Re_{crit} = 2100[1 + 12\delta^{1/2}]. \tag{23}$$

As $\delta \to 0$, the above equation reduces to the straight pipe $Re_{crit} = 2100$. In the present paper, the Reynolds numbers applied are much higher than those predicted by equation (23) to ensure that the flow in the helical pipe is within the turbulent regime.

NUMERICAL COMPUTATION

The governing equations have been solved with a Control-Volume Finite Element Method (CVFEM) similar to that introduced by Baliga and Patankar [19]. The FLUENT/UNS code [20] has been used as the numerical solver. As CVFEM combines the best aspects of the control-volume finite difference method (CVFDM) and the finite element method (FEM), it provides the mesh flexibility of FEM without sacrificing the benefits of CVFDM, which are robustness and economy.

An unstructured (block-structured) nonuniform grid system is used to discretize the governing equations. Figure 2 depicts the grid topology used on one cross-section and a typical hexahedral element for the three-dimensional grid system. As shown in Fig. 2, the three-dimensional hexahedral element has 27 nodes, with pressure stored on the eight vertex nodes and velocity components and scalars stored on the vertex, midedge, midface and center nodes.

The convection term in the governing equations was modeled with the bounded second-order upwind scheme and the diffusion term was computed using the multilinear interpolating polynomials $N_i(X, Y, Z)$ (also referred to as 'shape function' in FEM). The final discrete algebraic equation for variable ϕ at each node is a set of nominally linear equations that can be written as:

$$a_P \phi_P = \sum_{nb} a_{nb}\phi_{nb} + c_{sb} \tag{24}$$

where a_P is the center coefficient; a_{nb} is the influence coefficient for the neighbor; and c_{sb} is the contribution of the constant part of the source term S_c in $S = S_c + C_P\phi$ and of the boundary conditions. The SIMPLEC algorithm [21] is used to resolving the coupling between velocity and pressure. The algebraic equations are solved iteratively using an additive-correction multigrid method [22] with a Gauss–Seidel relaxation procedure. To accelerate convergence, the under-relaxation technique is applied to all dependent variables (the under-relaxation factor for p is 0.3; that

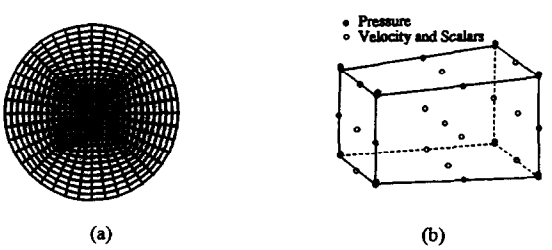

Fig. 2. Grid and nodes: (a) unstructured grid on one cross-section of the helical pipe; (b) nodes used for storage of dependent variables in the three-dimensional element.

Table 1. Grid independent tests ($Re = 2.5 \times 10^4$, $\delta = 0.050$, $\lambda = 0.2$)

Elements (sectional × axial)	$(T_b - T_0)/(T_w - T_b)$	$\Gamma_{eff,b}/\Gamma_l$	$Nu_{\theta,max}$	Nu_m
245 × 100	0.246	305.9	226.5	198.9
320 × 120	0.247	314.3	230.7	200.7
720 × 120	0.251	339.6	235.1	202.8
500 × 120	0.251	339.0	235.1	202.8
500 × 160	0.250	335.5	235.6	203.4
500 × 200	0.250	335.4	235.6	203.4

for T is 1.0; and that for u_j, k and ε is 0.7). The numerical computation is considered to be converged when the residual summed over all the computational nodes at nth iteration for variable ϕ, R^n_ϕ, satisfies the following criterion:

$$\frac{R^n_\phi}{R^m_\phi} \leqslant 10^{-5} \tag{25}$$

where ϕ applies for u_i, T, k and ε; and R^m_ϕ represents the maximum residual value after m iterations.

In the present study, the computational domain in the axial direction spreads from $\varphi = 0$–$270°$. The choice of this computational domain is based on the entry length data on curved pipes given by Austin and Seader [23] to ensure that fully developed flow results can be obtained on the outlet plane ($\varphi = 270°$). A grid refinement study was conducted to determine an adequate grid distribution. Table 1 presents a comparison of the predicted results at different grid distributions (sectional × axial) for a fully developed turbulent fluid flow in a helical pipe. The sectional number refers to the total number of elements on one cross section (φ = constant) of the pipe. The expression $\Gamma_{eff,b}/\Gamma_l$ is the ratio of bulk effective thermal conductivity to molecular thermal conductivity and $Nu_{\theta,max}$ is the maximum value of local Nusselt numbers along the circumference of the pipe. This table indicates that the 500×160 grid arrangement ensures a satisfactory solution for heat transfer in helical pipe. With the 500×160 and even finer grids, some computations were also repeated for fluid flow and heat transfer in helical pipes at lower δ, higher Re, of λ. It was observed that the difference in the solutions was in the order of about 1%. All the computations in this paper were carried out on a Sun 4/80 workstation in the Hemispheric Center for Environment Technology (HCET) at Florida International University (FIU). Approximately 350–400 iterations were needed in order to obtain the convergence results.

RESULTS AND DISCUSSION

Data comparison (fully developed heat transfer)

Due to the limited data on turbulent developing heat transfer in helical pipes, the present predictions are compared to previous studies on fully developed heat transfer in helical pipes with zero pitch (toroidal pipes). Figure 3 illustrates the comparison of present predictions of the fully developed Nusselt number with the experimental data reported by Rogers and Mayhew [4]. The experimental results of Rogers and Mayhew are well represented by the following empirical formula:

$$Nu_{fd} = 0.023 Re^{0.85} Pr^{0.4} \delta^{0.1}. \tag{26}$$

As can be observed, the numerical results agree fairly well with the measurements. Within the examined parameter ranges, the maximum difference between the present numerical results and the experimental data is approximately 5%. The discrepancies between the experimental and numerical results are considered to be caused mainly by the standard two-equation k–ε turbulence model. Also presented in Fig. 3 are the computed Nusselt numbers for turbulent heat transfer in a straight circular pipe. The agreement with the well-known Dittus–Boelter equation [24] is quite satisfactory:

$$Nu_{fd} = 0.023 Re^{0.8} Pr^{0.4}. \tag{27}$$

Development of turbulent thermal fields

The following numerical results were obtained under the inlet turbulence condition of $I = 5\%$, which is a typical turbulence level for turbulent pipe flows. The fluid physical properties were based on those for water with $Pr = 7.02$. The development of nondimensional temperature (Θ) fields in helical pipes is shown in Figs. 4 and 5. When the axial distance, s, is small, fluid of uniform temperature occupies most of the area of the cross-section. As s increases, the unbalanced centrifugal force of the main flow results in the shift of point of the maximum Θ to the outside of the pipe, forming steeper Θ gradients near the outer wall. When the heat transfer is fully developed, both the position shift and the magnitude of the maximum Θ reach their maximum.

Figures 4(a) ($\lambda = 0.0$) and 4(b) ($\lambda = 0.6$) illustrates the effects of λ on the developing nondimensional temperature fields for given Re and δ. When $\lambda = 0.0$, the turbulent temperature fields are asymmetric to the centerline connecting the outermost and innermost points of the cross-section. When $\lambda \neq 0$, the torsion caused by the finite pitch results in asymmetric developing turbulent temperature fields: the zones of higher values of Θ are rotated towards the bottom of the cross-section.

Figures 5(a) ($Re = 2.5 \times 10^4$) and 5(b) ($Re = 2.5 \times 10^5$) illustrate how Re affects the developing turbulent temperature fields for given δ and λ. At each axial location (s = constant), the value and pattern of the nondimensional temperature in most of the area of the cross-section are weakly influenced by the variation of Re. Compared with heat transfer at different Re (see below), it has been observed that a significant change in the temperature gradient occurs in the near wall region when Re varies.

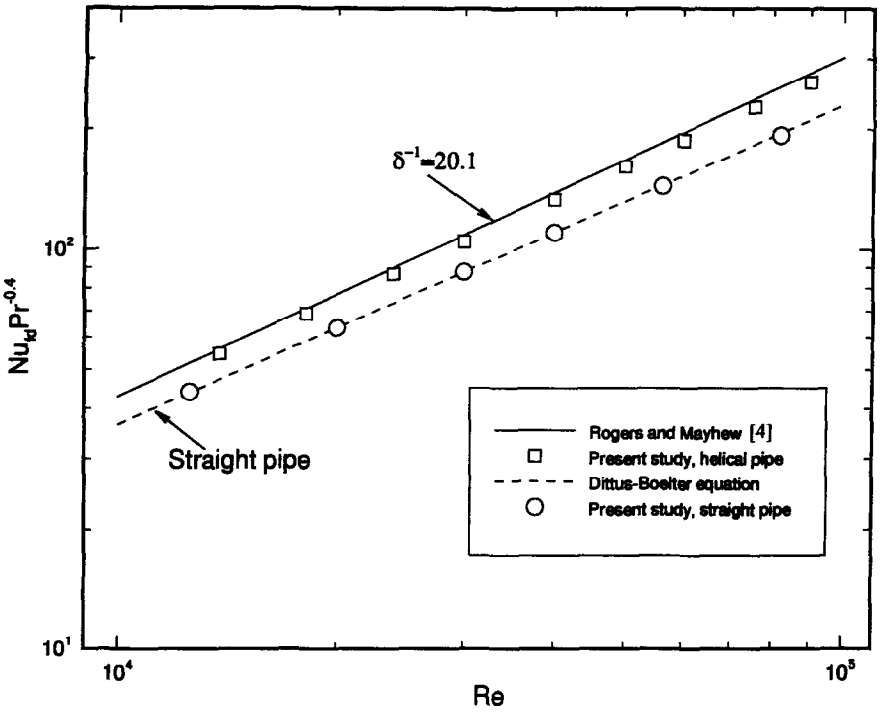

Fig. 3. Comparison of fully developed Nusselt numbers with experimental data. For helical pipe, $\lambda = 0$.

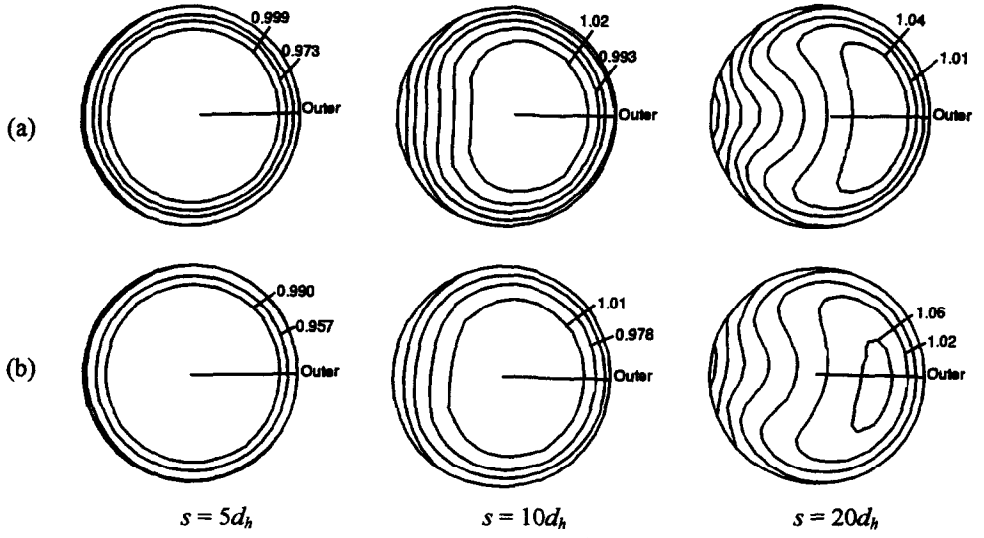

Fig. 4. Development of temperature fields at $Re = 2.5 \times 10^4$, $\delta = 0.025$: (a) $\lambda = 0.0$; (b) $\lambda = 0.6$.

Figures 4(b) ($\delta = 0.025$) and 5(a) ($\delta = 0.050$) reflect the influence of δ on developing turbulent temperature fields for given Re and λ. It is shown that when δ becomes larger, the development of the temperature field becomes faster and the shift of the fluid with higher Θ toward the outside becomes more significant.

Figures 6 and 7 show the development of the relative effective thermal conductivity (Γ_{eff}/Γ_l) fields in helical pipes. As the fluid turbulence develops from the inlet to the outlet, the effective thermal conductivity level is increased with the increase of s. In the course of the development, the maximum value of Γ_{eff}/Γ_l may vary non-monotonically due to the influence of finite pitch and curvature, but the value of the maximum Γ_{eff}/Γ_l at large s is definitely higher than that at small s. Figures 6(a) ($\lambda = 0.0$) and (b) ($\lambda = 0.6$) illustrates that the main effect of pitch is to rotate the zones of higher Γ_{eff}/Γ_l in a clockwise direction. Figures 7(a) ($Re = 2.5 \times 10^4$) and (b) ($Re = 2.5 \times 10^5$) indicates that the Γ_{eff}/Γ_l level is substantially increased when Re is increased. Figures 4(b) ($\delta = 0.025$) and

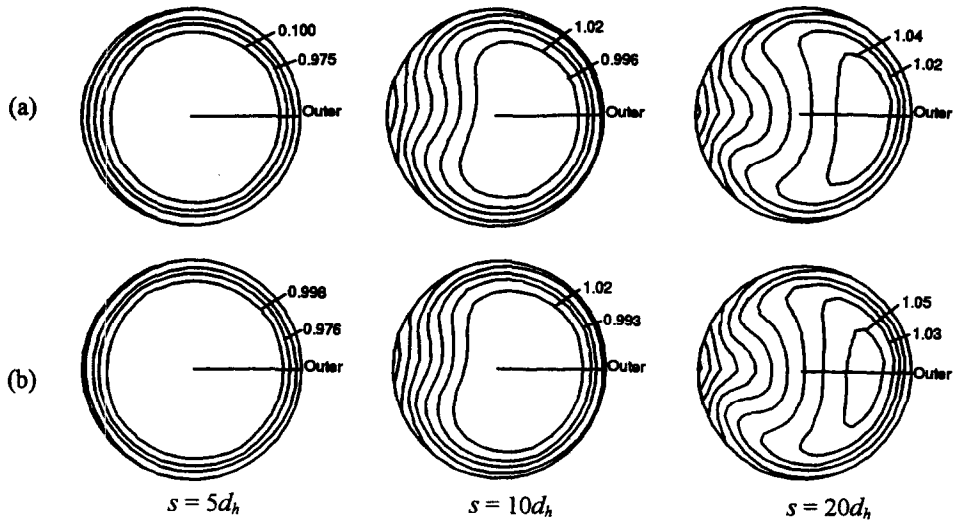

Fig. 5. Development of temperature fields at $\delta = 0.050$, $\lambda = 0.6$: (a) $Re = 2.5 \times 10^4$; (b) $Re = 1.0 \times 10^5$.

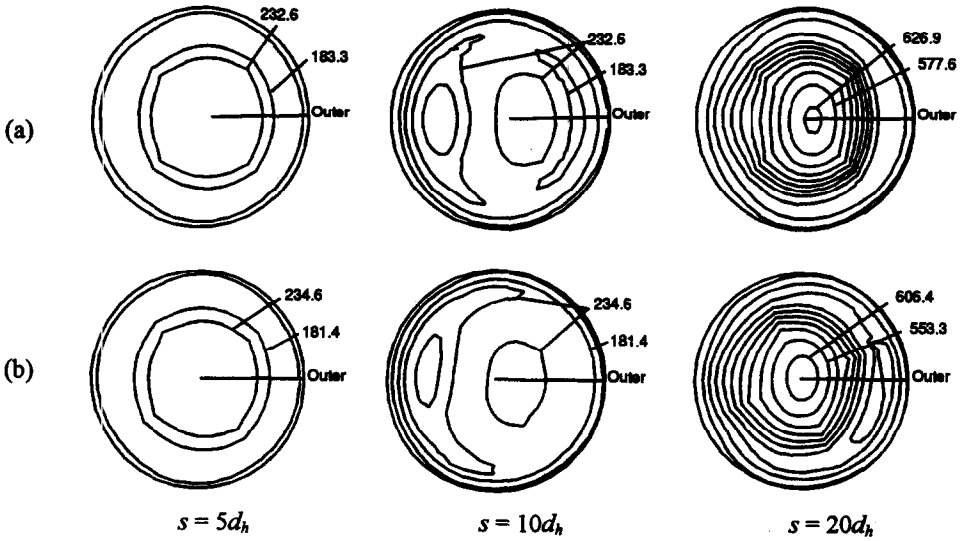

Fig. 6. Development of thermal conductivity fields at $Re = 2.5 \times 10^4$, $\delta = 0.025$: (a) $\lambda = 0.0$; (b) $\lambda = 0.6$.

5(a) ($\delta = 0.050$) demonstrates that zones of higher level $\Gamma_{\text{eff}}/\Gamma_l$ are shifted towards the outside of the pipe due to the increase of δ.

Development of the local Nusselt number

Figures 8 and 9 show the development of the local Nusselt number, Nu_θ, with the increase of s on the circumference of the helical pipe. The data are plotted in the direction from bottom ($r/a = -1.0$) to top ($r/a = 1.0$) of the pipe cross-section. For a cross-section at a given s, the higher and lower values of Nu_θ at $r/a = 0.0$ correspond to the Nusselt numbers at the outermost and innermost points of the pipe, respectively. It can be seen in the figures that at each s, the peripheral variation of Nu_θ is much steeper on the inner side than on the outer side. When s is small (near the inlet), the distribution of Nu_θ on the circumference is relatively smooth. As the flow proceeds downstream, the magnitude difference of Nu_θ between the outer and inner sides of the pipe increases.

When $\lambda = 0$ (Fig. 8(a)), the distribution of Nu_θ at each s is symmetric to the centerline ($r/a = 0.0$) connecting the innermost and outermost points of the pipe. There is a flat region around $r/a = 0.0$ with a relatively uniform variation of Nu_θ. The point of minimum Nu_θ is located at $r/a = 0.0$ on the inner side of the pipe. When $\lambda \neq 0$ (Figs 8(b) and 9(a,b), $\lambda = 0.6$), the distribution of Nu_θ is asymmetric to the centerline due to the effect of the finite pitch, especially at the later stage of heat transfer development. A step on the Nu_θ curve appears on the outer side of the pipe. The location of the minimum Nu_θ is found to be oscillatory about the innermost point with the increase of s.

The effect of δ on the development of Nu_θ is reflected in Figs 8(b) and 9(a). When δ increases, the variation of Nu_θ along the inner side of the pipe becomes steeper.

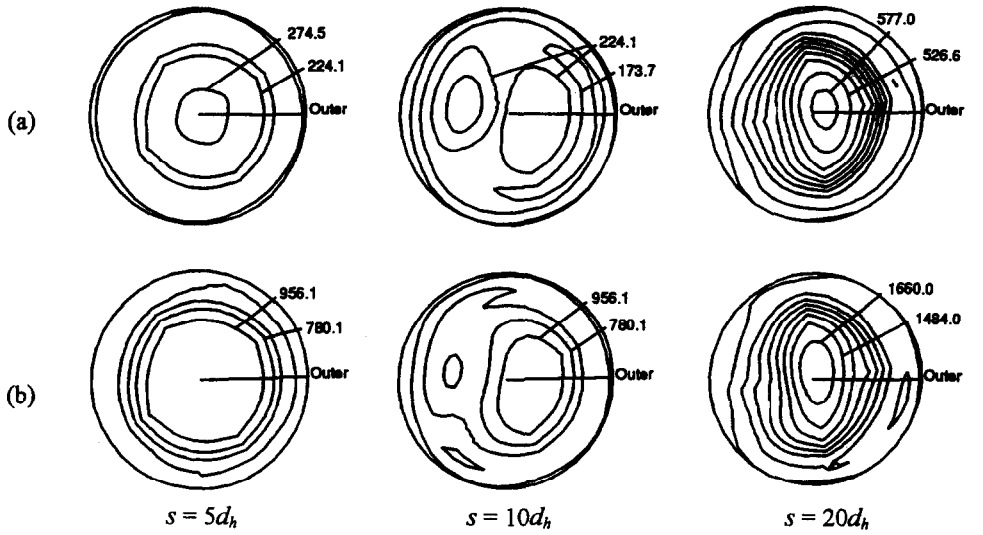

Fig. 7. Development of thermal conductivity fields at $\delta = 0.050$, $\lambda = 0.6$: (a) $Re = 2.5 \times 10^4$; (b) $Re = 1.0 \times 10^5$.

The 'step' on the Nu_θ curve in the middle region along the outer side of the pipe climbs.

Figures 9(a, b) (with a different scale for Nu_θ) demonstrate the effect of Re on the development of Nu_θ. When Re increases, both the magnitude of Nu_θ along the whole circumference of the pipe and the magnitude difference of Nu_θ between the outer and inner sides of the pipe decreases. The location of the minimum values of Nu_θ at each axial location remains almost unchanged with the increase of Re.

Development of the average Nusselt number

The development of the circumferential average Nusselt number, Nu_m, with axial location at different pitches, is depicted in Fig. 10. In the early developing stage ($s/d_h < 5$–8), Nu_m drops sharply as s/d_h increases due to the rapid development of the thermal boundary layer. After the early stage, Nu_m experiences an oscillatory state, in which the value of Nu_m is oscillatory with the variation of s/d_h before it is fully developed. Although the effect of λ is to reduce the magnitude of Nu_m in the fully developed stage, the magnitude of Nu_m at higher λ in the oscillatory stage may exceed that at lower λ, depending upon the axial location. For the case of smaller δ (Fig. 10(a)), one obvious peak value of Nu_m appears. The increase of λ results in the movement of the location of peak value of Nu_m downstream. For the case of larger δ (Fig. 10(b)), two obvious peak values of Nu_m are found. With the increase of λ, the oscillation of Nu_m tends to become significant. It has been ascertained that the oscillation of Nu_m is a consequence of the secondary flow in helical pipes. A similar oscillatory development of the Nusselt number was also found by both Liu [15] and Patankar *et al.* [25] in their parabolic numerical studies of laminar developing heat transfer in helical pipes, in which more peak values were found.

The effects of Re on the development of Nu_m are shown in Fig. 11 at two δ values. With the increase of Re, the magnitude of Nu_m at every axial location increases and the oscillation of Nu_m is strengthened. Numerical simulation also reveals that the axial locations of the peak values of Nu_m are affected very little by the variation of Re. Figure 11 also reveals that when δ is increased, the oscillation of Nu_m is enhanced. Except in the early developing stage, the effect of δ is to increase the magnitude of Nu_m at different axial locations on the helical pipes.

CONCLUSIONS

Three-dimensional turbulent developing heat transfer in helical pipes with finite pitch has been simulated with a control-volume finite element method. The fully elliptic numerical predictions of fully developed heat transfer are consistent with existing experimental data. As the turbulent flow develops downstream, the nonuniformity of the thermal fields increases. Except in the early developing stage, the development of turbulent thermal fields is influenced substantially by pitch, curvature ratio and Reynolds number.

The development of the local Nusselt number on the inner and outer sides of the helical pipes is found to be different. The location of the minimum values of the Nusselt number on the circumference of the pipe shifts as the flow proceeds downstream. The development of the circumferential average Nusselt number is found to be oscillatory before it is fully developed. When pitch, curvature, or Reynolds number increases, the oscillation phenomenon is enhanced.

Acknowledgements—The authors gratefully acknowledge the financial support of the National Science Foundation (NSF) under Grant no. CTS-9017732.

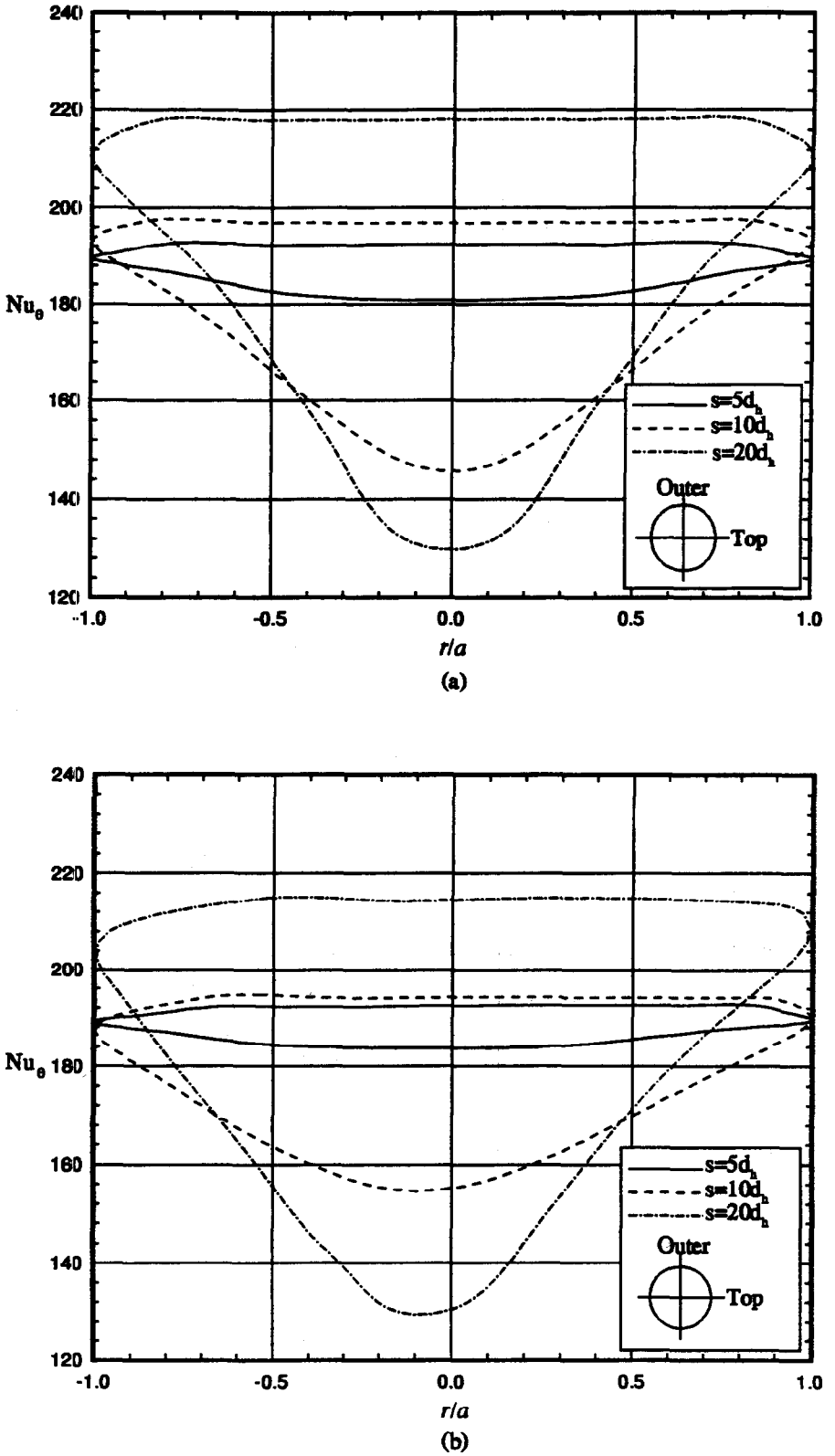

Fig. 8. Development of the local Nusselt number on the circumference of a helical pipe at $Re = 2.5 \times 10^4$, $\delta = 0.025$: (a) $\lambda = 0.0$; (b) $\lambda = 0.60$.

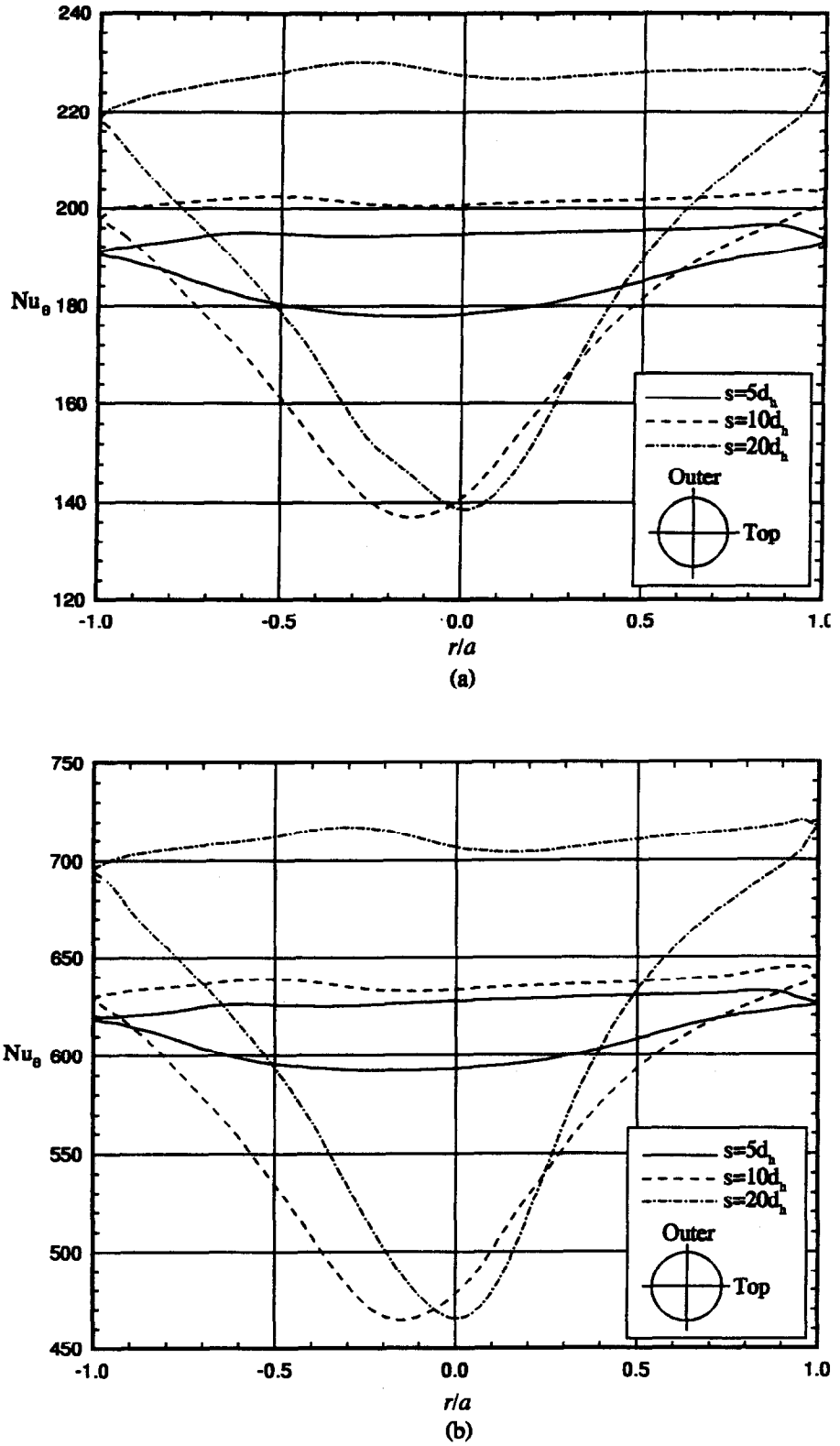

Fig. 9. Development of the local Nusselt number on the circumference of a helical pipe at $\delta = 0.050$, $\lambda = 0.6$: (a) $Re = 2.5 \times 10^4$; (b) $Re = 1.0 \times 10^5$.

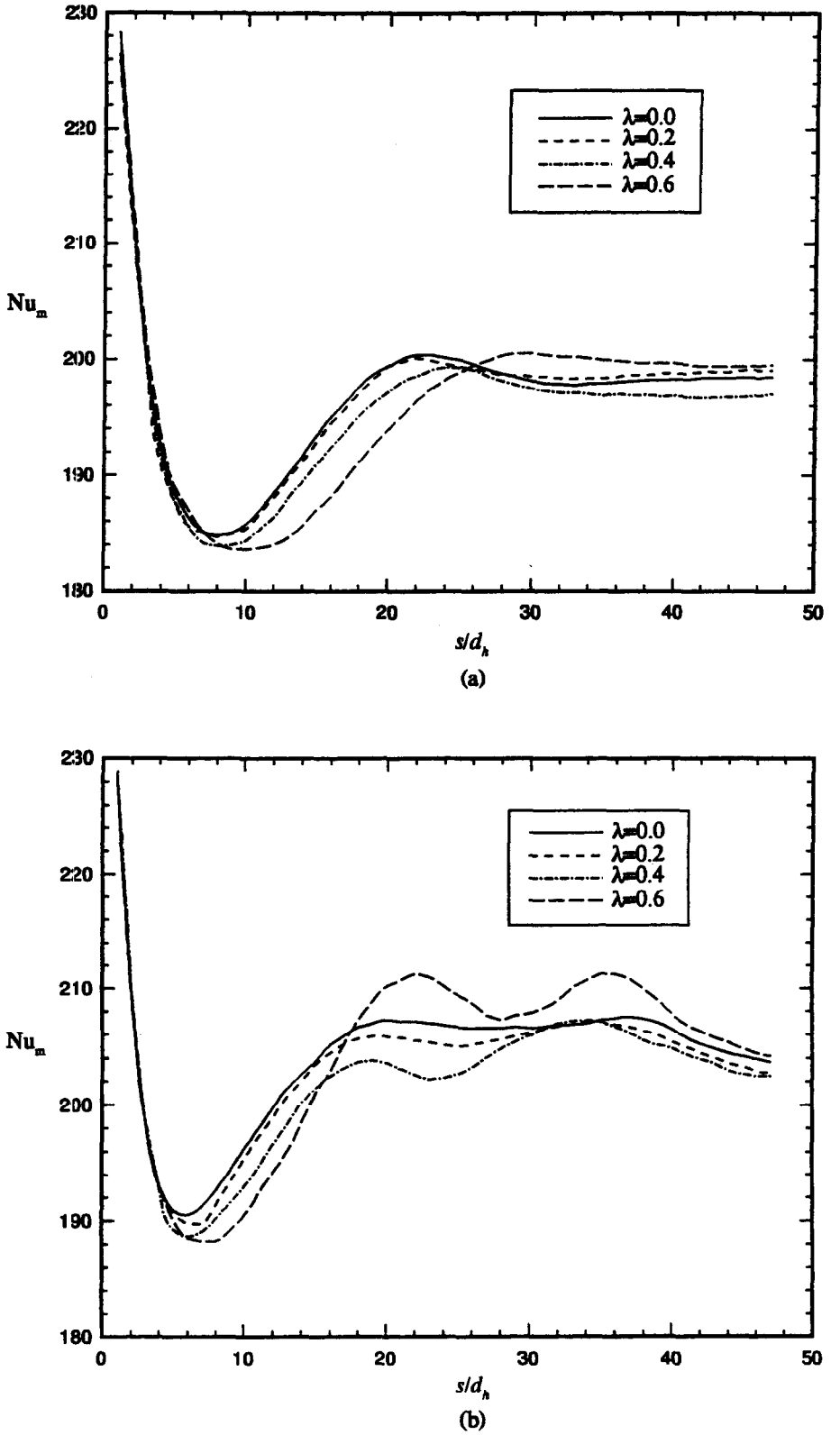

Fig. 10. Effects of pitch on the development of the average Nusselt number at $Re = 2.5 \times 10^4$: (a) $\delta = 0.025$; (b) $\delta = 0.050$.

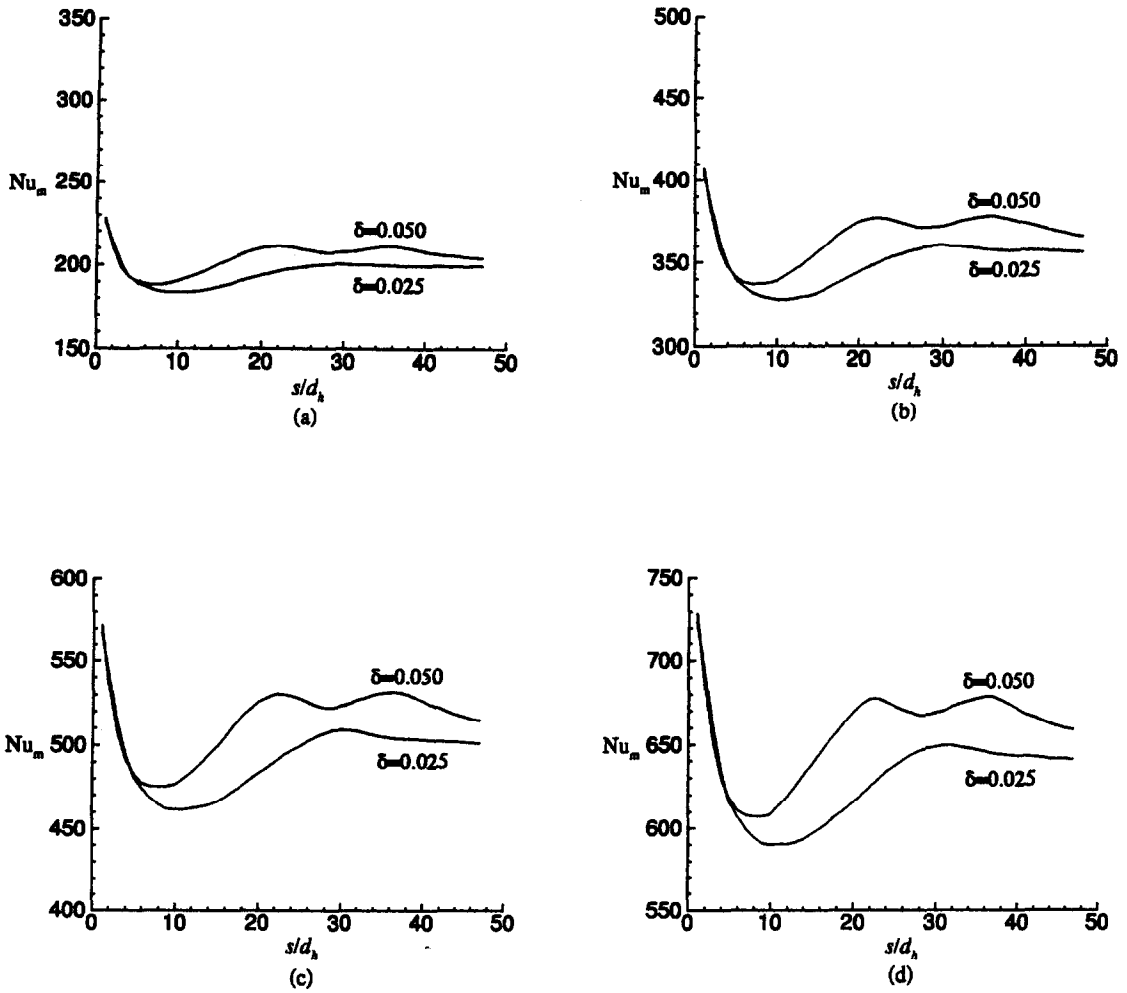

Fig. 11. Effects of the Reynolds number on the development of the average Nusselt number at $\lambda = 0.6$: (a) $Re = 2.5 \times 10^4$; (b) $Re = 5.0 \times 10^4$; (c) $Re = 7.5 \times 10^4$; (d) $Re = 1.0 \times 10^5$.

REFERENCES

1. Berger, S. A., Talbot, L. and Yao, L. S., Flow in curved pipes. *Annual Review of Fluid Mechanics*, 1983, **15**, 461–512.
2. Shah, R. K. and Joshi, S. D., Convective heat transfer in curved ducts. In *Handbook of Single-Phase Convective Heat Transfer*, S. Kakac, R. K. Shah and W. Aung, Chapter 5. Wiley, New York, 1987.
3. Seban, R. A. and McLaughlin, E. F., Heat transfer in tube coils with laminar and turbulent flow. *International Journal of Heat and Mass Transfer*, 1963, **6**, 387–395.
4. Rogers, G. F. C. and Mayhew, Y. R., Heat transfer and pressure loss in helically coiled tubes with turbulent flow. *International Journal of Heat and Mass Transfer*, 1964, **7**, 1207–1216.
5. Hogg, G. W., The effect of secondary flow on point heat transfer coefficients for turbulent flow inside curved tubes. Ph.D. thesis, University of Idaho, 1968.
6. Mori, Y. and Nakayama, W., Study on forced convection heat transfer in curved pipes (2nd report, turbulent region). *International Journal of Heat and Mass Transfer*, 1967, **10**, 37–59.
7. Kalb, C. E. and Seader, J. D., Entrance region heat transfer in a uniform wall-temperature helical coil with transition from turbulent to laminar flow. *International Journal of Heat and Mass Transfer*, 1983, **26**, 23–32.
8. Mikaila, V. A. and Poskas, P. S., Local heat transfer in coiled tubes at high heat fluxes (1. Experimental unit, technique and results of preliminary experiments). *Heat Transfer—Soviet Research*, 1990, **22**, 713–727.
9. Rao, B. K., Turbulent heat transfer to viscoelastic fluids in helical passages. *Experimental Heat Transfer*, 1993, **6**, 189–203.
10. Rao, B. K., Turbulent heat transfer to power-law fluids in helical passages. *International Journal of Heat and Mass Transfer*, 1994, **15**, 142–148.
11. Patankar, S. V., Pratap, V. S. and Spalding, D. B., Prediction of turbulent flow in curved pipes. *Journal of Fluid Mechanics*, 1975, **67**(3), 583–595.
12. Yang, G. and Ebadian, M. A., Turbulent forced convection in a helicoidal pipe with substantial pitch. *International Journal of Heat and Mass Transfer*, 1995, **39**, 2015–2022.
13. Patankar, S. V. and Spalding, D. B., A calculation procedure for heat, mass and momentum transfer in three-dimensional parabolic flows. *International Journal of Heat and Mass Transfer*, 1972, **15**, 1787–1806.
14. Germano, M., On the effect of the torsion in a helical pipe flow. *Journal of Fluid Mechanics*, 1982, **125**, 1–8.
15. Liu, S., Laminar flow and heat transfer in helical pipes with finite pitch. Ph.D. thesis, University of Alberta, Canada, 1992.
16. Launder, B. E. and Spalding, D. B., *Mathematical Models of Turbulence*. Academic Press, London, 1972.

17. Launder, B. E. and Spalding, D. B., The numerical computation of turbulent flows. NTIS N74-12066, Imperial College of Science and Technology, 1973.
18. Srinivasan, P. S., Nandapurkar, S. and Holland, F. A., Friction factor for coils. *Transactions of the Institute of Chemical Engineers*, 1970, **48**, T156-T161.
19. Baliga, B. R. and Patankar, S. V., A control volume finite-element method for two-dimensional fluid flow and heat transfer. *Numerical Heat Transfer*, 1983, **6**, 245–261.
20. *FLUENT/UNS User's Guide*, release 1.0, Fluent Inc., Lebanon, NH, 1994.
21. Doormaal, J. and Raithby, G. D., Enhancements of the SIMPLE method for predicting incompressible flow problems. *Numerical Heat Transfer*, 1984, **7**, 147–158.
22. Hutchinson, B. R. and Raithby, G. D., A multigrid method based on the additive correction strategy. *Numerical Heat Transfer*, 1986, **9**, 511–537.
23. Austin, L. R. and Seader, J. D., Entry region for steady viscous flow in coiled circular pipes. *AIChE Journal*, 1974, **20**, 820–822.
24. Dittus, F. W. and Boelter, L. M. K., Heat transfer in automobile radiators of the tubular type. *University of California Publ. Engineering*, 1930, **2**, 443–461.
25. Patankar, S. V., Pratap, V. S. and Spalding, D. B., Prediction of laminar flow and heat transfer in helically coiled pipes. *Journal of Fluid Mechanics*, 1974, **62**(3), 539–551.